

GLOBAL CLUSTER SYSTEMS AND THE MISSING SATELLITE PROBLEM: IMPLICATIONS FOR COLD DARK MATTER MODELS

PATRICK CÔTÉ

Department of Physics and Astronomy, Rutgers University, New Brunswick, NJ 08854; pcote@physics.rutgers.edu

MICHAEL J. WEST

Department of Physics and Astronomy, University of Hawaii, Hilo, HI 96720; west@bohr.uhh.hawaii.edu

AND

RONALD O. MARZKE

Department of Physics and Astronomy, San Francisco State University, 1600 Holloway Avenue, San Francisco, CA 94132; marzke@quark.sfsu.edu

Received 2001 October 2; accepted 2001 November 23

ABSTRACT

We analyze the metallicity distributions of globular clusters belonging to 28 early-type galaxies in the survey of Kundu & Whitmore. A Monte Carlo algorithm that simulates the chemical evolution of galaxies that grow hierarchically via dissipationless mergers is used to determine the most probable protogalactic mass function for each galaxy. Contrary to the claims of Kundu & Whitmore, we find that the observed metallicity distributions are in close agreement with the predictions of such hierarchical formation models. The mass spectrum of protogalactic fragments for the galaxies in our sample has a power-law behavior, $n(M) \propto M^\alpha$, with an index of $\alpha \simeq -2$. This spectrum is indistinguishable from the mass spectrum of dark matter halos predicted by cold dark matter models for structure formation. We argue that these protogalactic fragments—the likely sites of globular cluster formation in the early universe—are the disrupted remains of the “missing” satellite galaxies predicted by cold dark matter models. Our findings suggest that the solution to the missing satellite problem is through the suppression of gas accretion in low-mass halos after reionization, or via self-interacting dark matter, and argue against models with suppressed small-scale power or warm dark matter.

Subject headings: cosmology: observations — dark matter — galaxies: elliptical and lenticular, cD — galaxies: formation — galaxies: star clusters

1. INTRODUCTION

Cold dark matter (CDM) models offer an attractive theory for the formation of cosmological structure. These models, and particularly the Λ CDM variant, show impressive self-consistency with many of the most fundamental astrophysical observations: i.e., the expansion age of the universe, the primordial element abundance, the two-point correlation function of cluster and galaxies, the local space density and redshift evolution of massive clusters, and the large-scale streaming motions of galaxies in the local universe (e.g., Bahcall et al. 1999). Nevertheless, it has become clear that this success on large scales (i.e., $R \gtrsim 0.1$ –1 Mpc) does not extend to the level of galaxies (see, e.g., Sellwood & Kosowsky 2002 for a review). Simply stated, CDM models produce an overabundance of power on small scales when normalized to match the observed large-scale power: e.g., the models yield dark matter density profiles that are steeper than those observed (Flores & Primak 1994) and overpredict the number of dwarf galaxies (Kauffmann, White, & Guideroni 1993). We examine the latter issue—the so-called missing satellite problem—by using the globular clusters (GCs) associated with a sample of nearby, early-type galaxies to derive the mass distribution of accreted material in these systems.

Most recent attempts to explain the missing satellite problem have focussed on the properties of the dark matter itself. Competing models suggest that the dark matter is warm (Colín, Avila-Reese, & Valenzuela 2000), decaying (Cen 2001), self-interacting (Davé et al. 2001), repulsive (Goodman 2000), or annihilating (Riotto & Tkachev 2000). Alternatively, the standard CDM picture may be modified

to include a broken scale invariance that suppresses small-scale power (Kamionkowski & Liddle 2000). Yet another modification has been proposed by Bullock, Kravtsov, & Weinberg (2000), who note that a photoionizing background is expected to inhibit the accretion of gas onto low-mass halos after the epoch of reionization. In this latter scenario, small-scale power is not suppressed, but *hidden*: as a mixed population of disrupted and surviving dark-matter-dominated subhalos.

In what follows, we present a simple technique for measuring the mass distribution of disrupted subhalos in low-redshift galaxies. Our technique relies on the GC systems of these galaxies, which, by virtue of their extreme age and apparently universal formation efficiency, represent ideal tracers of the original population of low-mass subhalos or, in the terminology used here, protogalactic fragments. The observational database consists of GC color and metallicity distributions for 28 early-type galaxies presented by Kundu & Whitmore (2001). Although most cosmological evidence appears to favor the notion that the GC systems of large galaxies were assembled hierarchically (e.g., see Gnedin, Lahav, & Rees 2001 and references therein), Kundu & Whitmore (2001) claim that the GC metallicity distributions of their program galaxies are incompatible with such scenarios. In this paper, we analyze the data of Kundu & Whitmore (2001) using a quantitative numerical technique, described in a pair of earlier papers (Côté, Marzke, & West 1998; Côté et al. 2001), which is designed to recover the protogalactic mass spectrum of a galaxy. The method assumes that the mergers and accretions that cause galaxies to grow hierarchically induce little or no gas dissipation.

The mass spectra that we derive for the protogalactic fragments in each of these galaxies are indistinguishable from those predicted by CDM models for the population of low-mass dark matter halos, a finding that has obvious implications for the missing satellite problem.

2. GLOBULAR CLUSTER DATA

Since GCs as a class are composed of coeval stars, the interpretation of their broadband colors is far more straightforward than is the case for galaxies. Moreover, for composite stellar populations with mean ages of a few gigayears or more, broadband colors are primarily sensitive to metallicity, not age (Bruzual & Charlot 1993; Worthey 1994). Luckily, the great majority of the GCs in these systems appear to be older than this according to optical spectroscopy, color-magnitude diagrams, and luminosity function turnover magnitudes for GCs belonging to nearby dwarf elliptical, dwarf spheroidal, spiral and giant elliptical galaxies (e.g., Buonanno et al. 1998; Layden & Sarajedini 1997; Harris, Poole & Harris 1998; Cohen, Blakeslee, & Rhyzov 1998; Puzia et al. 1999; Lee & Kim 2000; Beasley et al. 2000; Larsen et al. 2001). Indeed, evidence from various sources (see Gnedin et al. 2001) points to minimum GC ages in the range $8 \lesssim t \lesssim 12$ Gyr, suggesting that, in the currently fashionable Λ CDM models, the bulk of GC formation in early-type galaxies had occurred *before* $1 \lesssim z \lesssim 4$. Thus, for the early-type galaxies considered here, we may be confident that the observed GC colors are reliable metallicity indicators.

Several recent studies have reported color/metallicity distributions for the GC systems of early-type galaxies based on archival *HST* data (e.g., Gebhardt & Kissler-Patig 1999; Kundu & Whitmore 2001; Larsen et al. 2001). As noted by van den Bergh (2001), the GC systems of these galaxies exhibit “a bewildering variety of characteristics.” This is particularly true of their metallicity distributions, which range from obviously multimodal systems to those with a single (metal-rich or metal-poor) peak. This remarkable variety has led some investigators to suggest that no single recipe for galaxy formation is capable of explaining the full range in GC properties (e.g., Harris 2000). Indeed, there is clear supporting evidence for most of the models that seek to explain the formation of GC systems and their host galaxies: e.g., the formation of massive clusters in gas-rich mergers (e.g., Whitmore & Schweizer 1995) and the acquisition of GCs through dissipationless accretions (e.g., Ibata, Gilmore, & Irwin 1994). The most immediate question is which—if any—of these processes has dominated the formation of the GC systems that we observe today.

In what follows, we model these diverse GC metallicity distributions using a simple prescription for hierarchical galaxy formation, described more fully in § 3. In the interests of homogeneity, we limit ourselves to the GC color and metallicity distributions for 28 early-type galaxies presented in Kundu & Whitmore (2001). Their galaxy sample is $\sim 60\%$ larger than that of Larsen et al. (2001), while the number of detected GCs per galaxy is $\sim 50\%$ larger than that of Gebhardt & Kissler-Patig (1999) for galaxies appearing in both studies. A single galaxy in the Kundu & Whitmore sample, NGC 4486B, has been excluded from the analysis since the modeling of its GC metallicity distribution is complicated by the fact that a significant fraction of its initial mass has probably been tidally stripped by NGC 4486 (e.g., Faber 1973; Kormendy et al. 1997).

Kundu & Whitmore (2001) present *VI* photometry and $(V-I)$ colors for GC candidates associated with each of their program galaxies. The number of GCs, N_{GC} , ranges between 445 for NGC 4649 and 41 for NGC 5845, with a mean of $\langle N_{\text{GC}} \rangle = 163$. Since our goal is to model the detailed shape of the observed GC metallicity distributions, we restrict ourselves to GCs with colors measured to a precision of $\sigma(V-I) = 0.2$ mag or better—roughly the separation between the metal-rich and metal-poor peaks in the most luminous galaxies. With this selection criterion, the number of GCs per galaxy ranges from 404 in NGC 4649 to 41 in NGC 5845, with a mean value of $\langle N_{\text{GC}} \rangle = 144$. The adopted GC color-metallicity relation is that of Kissler-Patig et al. (1998),

$$[\text{Fe}/\text{H}] = -4.50 + 3.27(V-I), \quad (1)$$

which is based on a combined sample of GCs in the Milky Way and NGC 1399 with measured metallicities. Although there is significant scatter about this best-fit relation (see Fig. 13 of Kissler-Patig et al. 1998), our conclusions are largely insensitive to the exact choice of color-metallicity relation. The clusters used to establish this relation have metallicities in the range $-2.4 \lesssim [\text{Fe}/\text{H}] \lesssim +0.3$ dex ($0.64 \lesssim V-I \lesssim 1.47$ mag), an interval that includes the vast majority of clusters considered here.

To simulate the metallicity distribution of a GC system, we require an estimate of the host galaxy’s luminosity, and hence distance. In principal, it is possible to measure individual galaxy distances from the GC data themselves, using the observed turnover of the GC luminosity function (GCLF). Unfortunately, Kundu & Whitmore (2001) were able to obtain reliable two-parameter GCLF fits (i.e., turnover magnitude and dispersion) for just 10 of their 28 galaxies. As a consequence, distances for their program galaxies were taken primarily from early versions of the surface brightness fluctuation (SBF) survey of Tonry and collaborators, with extinction estimates from Burstein & Heiles (1984). Recently, the final version of the SBF catalog—based on an improved calibration—has become available (Tonry et al. 2001), so we adopt the latest SBF distances for the sample galaxies. Likewise, improved extinctions for all 28 galaxies have been calculated from the Schlegel, Finkbeiner, & Davis (1998) DIRBE maps. Unfortunately, two of the sample galaxies—NGC 7626 and NGC 5982—are not included in Tonry et al. (2001) catalog. For NGC 7626, we have combined the Schlegel et al. (1998) extinction with the Tully-Fisher distance for the Pegasus group from Sakai et al. (2000) to find a true distance modulus of 33.73 mag. This is significantly larger than the value of 33.01 adopted by Kundu & Whitmore based on the fundamental plane distance of Prugniel & Simien (1996). For NGC 5982, no recent distance determination is available, so we follow Kundu & Whitmore in adopting the Prugniel & Simien (1996) distance for this galaxy, but corrected for our new extinction. Because of these revised distances and extinctions, the absolute magnitudes of the program galaxies differ from those reported in Kundu & Whitmore. The mean magnitude difference is $\langle \Delta M_V \rangle = 0.18 \pm 0.08$ mag (mean error), in the sense that our magnitudes are brighter than those of Kundu & Whitmore. The largest discrepancies are found for NGC 5813, NGC 7626, and IC 1459, whose absolute magnitudes have become brighter by $\Delta M_V \sim 0.9$ mag.

Observational data for the sample galaxies are sum-

marized in Table 1. From left to right, the first six columns in this table report the galaxy name, integrated V -band magnitude from NED, extinction from Schlegel et al. (1998), adopted distance modulus (uncorrelated for V -band absorption, A_V , absolute visual magnitude, and total number of GCs having $\sigma(V-I) \leq 0.2$ mag. The remaining columns are discussed in detail below.

3. NUMERICAL METHOD

3.1. Model Input

We model the observed GC color and metallicity distributions for our program galaxies using a numerical code that has been described in two previous papers. The first of these papers (Côté et al. 1998) outlined the strategy for simulating GC color and metallicity distributions of galaxies that grow hierarchically via dissipationless mergers, and applied the method to the observed GC metallicity distribution of the giant elliptical galaxy NGC 4472, one of the objects in the current sample. A number of refinements to this original code were described in Côté et al. (2000), where the model was extended to the GC systems and halo field stars of spiral galaxies (i.e., the Milky Way and M31). Since a complete discussion of the approach may be found in these papers, we give only a brief outline here.

The method uses an empirical, Monte Carlo approach to simulate the metallicity distributions of GCs associated with the end products of multiple dissipationless mergers and accretions, as expected in hierarchical models in which

the *bulk* of GC (and star) formation takes place in distinct protogalactic fragments and occurs *prior* to the epoch of galaxy assembly.¹ Using a Monte Carlo approach, it is possible to simulate the GC metallicity distribution of an individual galaxy by specifying three model ingredients: (1) an assumed form for the mass or luminosity function of the protogalactic fragments which agglomerate into the final galaxy; (2) a relation between the mass or luminosity of the protogalactic fragment and the mean metallicity of its GC system; and (3) the number of GCs per unit protogalactic fragment mass or luminosity. Each of these ingredients is determined empirically from observations of the GC systems of low-redshift galaxies. This empirical approach has the important practical advantage that it avoids the uncertainties involved in modeling directly the cycle of gas cooling, star formation, and feedback in these halos (issues which, ultimately, must be addressed in any complete theory of GC formation). As discussed in Côté et al. (1998), the merging probability of protogalactic fragments is assumed to be independent of mass. As Figure 1 of Bullock et al. (2000) shows for the specific case of the Milky Way, this assumption appears remarkably sound for protogalactic fragments with circular velocities of less than $v_c \simeq 60$ km s⁻¹, corresponding to a mass of $M \sim$ a few times $10^9 M_\odot$.

¹ Strictly speaking, the process is dissipationless only in the sense that the formation of GCs—clearly a dissipative process—is not driven by the mergers themselves, but rather by the cooling and collapse of gas within each protogalactic fragment.

TABLE 1
PROTOGALACTIC MASS FUNCTIONS OF EARLY-TYPE GALAXIES DEDUCED FROM THEIR GLOBULAR CLUSTER SYSTEMS

Galaxy	V_T (mag)	$E(V-I)$ (mag)	$5 \log d - 5 + A_V$ (mag)	M_V (mag)	N_{GC}	χ^2	α	ζ
NGC 4472.....	8.41	0.030	31.06	-22.72	338	1.61	-1.85 ± 0.10	0.30 ± 0.05
NGC 4649.....	8.84	0.037	31.13	-22.38	404	0.65	-1.90 ± 0.10	0.35 ± 0.05
NGC 4406.....	8.90	0.039	31.17	-22.37	181	0.78	$-2.00^{+0.15}_{-0.05}$	0.10 ± 0.05
NGC 4365.....	9.56	0.029	31.55	-22.06	280	0.67	-1.65 ± 0.15	$0.10^{+0.15}_{-0.05}$
NGC 5322.....	10.23	0.016	32.47	-22.29	118	0.39	$-1.95^{+0.15}_{-0.05}$	0.30 ± 0.1
NGC 4494.....	9.83	0.029	31.16	-21.40	123	0.46	-2.00 ± 0.05	$0.15^{+0.15}_{-0.10}$
NGC 7626 ^a	11.11	0.099	33.73	-22.86	111	0.44	$-1.60^{+0.15}_{-0.10}$	0.10 ± 0.05
NGC 5982 ^b	11.13	0.022	32.87	-21.75	61	0.39	$-1.95^{+0.25}_{-0.10}$	0.40 ± 0.15
IC 1459.....	9.99	0.022	32.38	-22.39	172	0.86	$-1.95^{+0.05}_{-0.10}$	$0.30^{+0.10}_{-0.05}$
NGC 3610.....	10.84	0.014	31.68	-20.84	107	0.62	$-1.95^{+0.05}_{-0.10}$	$0.45^{+0.10}_{-0.05}$
NGC 584.....	10.48	0.057	31.66	-21.18	112	0.69	$-1.90^{+0.20}_{-0.10}$	$0.35^{+0.10}_{-0.15}$
NGC 4621.....	9.63	0.024	31.42	-21.79	165	0.42	$-1.65^{+0.05}_{-0.10}$	0.25 ± 0.05
NGC 4552.....	9.75	0.056	31.07	-21.32	196	1.11	$-2.00^{+0.20}_{-0.05}$	$0.10^{+0.45}_{-0.05}$
NGC 5813.....	10.46	0.076	32.73	-22.27	185	0.96	-2.00 ± 0.05	0.10 ± 0.05
NGC 4589.....	10.73	0.038	31.80	-21.07	134	1.03	$-1.95^{+0.15}_{-0.10}$	0.25 ± 0.05
NGC 4278.....	10.16	0.038	31.12	-20.96	244	1.32	-2.00 ± 0.05	$0.30^{+0.05}_{-0.10}$
NGC 4473.....	10.20	0.038	31.07	-20.87	145	0.44	$-2.00^{+0.10}_{-0.05}$	0.30 ± 0.10
NGC 3379.....	9.28	0.033	30.20	-20.92	63	0.44	$-1.90^{+0.15}_{-0.10}$	0.35 ± 0.10
NGC 821.....	10.68	0.143	32.26	-21.58	101	1.19	$-2.00^{+0.10}_{-0.05}$	$0.10^{+0.10}_{-0.05}$
NGC 3608.....	10.76	0.029	31.87	-21.11	95	1.29	$-1.95^{+0.20}_{-0.10}$	0.10 ± 0.05
NGC 4291.....	11.47	0.050	32.21	-20.74	138	0.84	$-1.95^{+0.15}_{-0.10}$	0.10 ± 0.05
NGC 1439.....	11.39	0.041	32.23	-20.84	85	1.08	$-1.80^{+0.40}_{-0.20}$	$0.10^{+0.10}_{-0.05}$
NGC 1427.....	10.86	0.018	31.90	-21.04	146	0.54	$-2.00^{+0.20}_{-0.05}$	$0.20^{+0.10}_{-0.15}$
NGC 3377.....	10.38	0.046	30.36	-19.98	106	0.35	$-1.80^{+0.45}_{-0.15}$	$0.40^{+0.10}_{-0.05}$
NGC 4550.....	11.68	0.057	31.13	-19.45	47	0.83	$-1.75^{+0.50}_{-0.30}$	0.20 ± 0.15
NGC 5845.....	12.48	0.073	32.24	-19.76	41	0.35	$-1.75^{+0.35}_{-0.30}$	$0.35^{+0.25}_{-0.15}$
NGC 4660.....	11.24	0.048	30.64	-19.40	98	0.53	-1.65 ± 0.15	$0.25^{+0.10}_{-0.05}$
NGC 4458.....	12.07	0.033	31.26	-19.19	43	0.44	-1.75 ± 0.25	$0.70^{+0.10}_{-0.05}$
Mean						Mean	-1.88 ± 0.03	0.25 ± 0.03

^a Tully Fisher distance for the Pegasus group from Sakai et al. (2000).

^b Fundamental Plane distance from Prugniel & Simien (1996).

The luminosity function of protogalactic fragments is parameterized as a Schechter function,

$$n(L) \propto (L/L^*)^\alpha \exp(-L/L^*), \quad (2)$$

where L^* is a characteristic luminosity and α is an exponent that governs the relative number of faint and bright systems (Schechter 1976). Note that the luminosity in equation (2) refers to the *present day* luminosity of surviving protogalactic fragments (i.e., isolated galaxies of low- and intermediate-luminosity; Larson 1988). Over the luminosity range considered here, we assume a constant V -band mass-to-light ratio of $Y_V = 5$ at $z = 0$, which is roughly appropriate for the low- and intermediate-luminosity galaxies used below to define the relation between mean GC metallicity and host galaxy luminosity (Mateo 1998). We take the low-luminosity cutoff in equation (2) to be $L_V = 1.6 \times 10^7 L_{V,\odot}$, or $M = 8 \times 10^7 M_\odot$. These limits correspond to the Fornax dSph galaxy (the faintest galaxy known to contain its own GC system), but the precise choice has little effect on the calculated GC metallicity distributions for slopes shallower than $\alpha = -2$. At the bright end, we adopt a constant value of $L_V^* = 2 \times 10^{10} L_{V,\odot}$ for all simulations (Côté et al. 2000), while α is a free parameter to be determined on a galaxy-by-galaxy basis through a comparison of the observed and simulated GC metallicity distributions. Note that, for masses less than $M \sim 10^{11} M_\odot$, the protogalactic mass function has a nearly power-law form,

$$n(M) \propto (M/M^*)^\alpha, \quad (3)$$

which is also characteristic of the extended Press-Schechter mass functions used in semianalytic models. Our decision to treat the change in the initial luminosity and mass functions as a change in α alone is clearly an approximation, as L^* and M^* must unavoidably increase in the presence of mergers and accretions. Although our simulations have no time resolution, cosmological N -body simulations demonstrate that the change in M^* should have only a modest effect on the final GC metallicity distribution: Figure 12 of Pearce et al. (2001) suggests that change in the high-end cutoff of the mass function between $z = 3$ and $z = 0.2$ is about a factor of 4, corresponding to a maximum shift in $\langle V-I \rangle$ color of 0.08 mag for the highest mass protogalactic fragments.

The relation between GC metallicity and luminosity/mass of the host protogalactic fragment has been discussed extensively in Côté et al. (2000). Figure 1 shows the mean GC metallicity plotted against the luminosity (or mass) of nine dwarf elliptical (dE) and dwarf spheroidal (dSph) galaxies (circles), with data taken directly from that paper. Triangles indicate the metal-rich GC systems of two well-studied spiral galaxies: the Milky Way and M31. In both cases, the luminosities and masses refer to their *bulges*; that is to say, we assign the metal-rich GCs in these galaxies to their bulge components, and not their disks (Minniti 1995; Côté 1999). Our estimate for the relation between the mean GC color and the absolute magnitude of the host protogalactic fragment is

$$\langle V-I \rangle = 0.04 - 0.055 M_V, \quad (4)$$

which is indicated by the dashed line in Figure 1. This “zero-age” relation gives the dependence of mean GC color on the luminosity, or mass, of the progenitor protogalactic

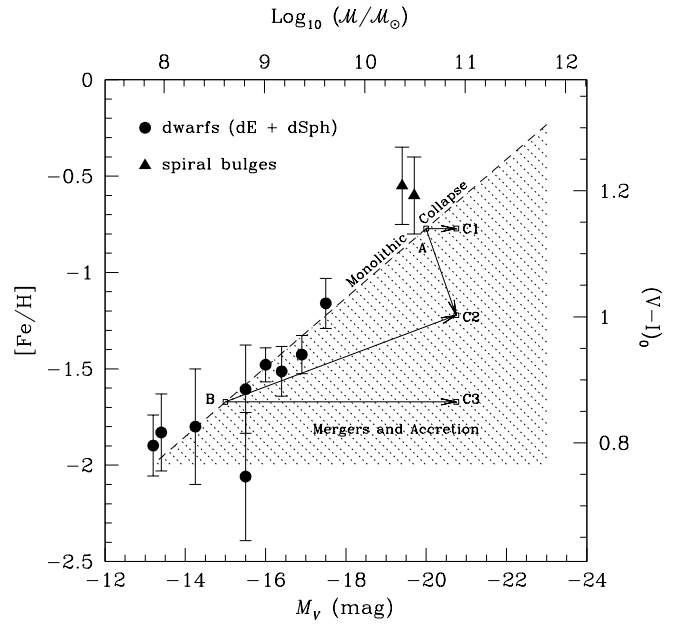


FIG. 1.—Mean color and metallicity of globular clusters belonging to low- and intermediate-luminosity galaxies, plotted as a function of absolute galaxy magnitude (circles). Triangles show the metal-rich globular cluster populations of the Milky Way and M31, plotted against their respective bulge luminosities. The tightness of this correlation indicates that the chemical enrichment of the globular clusters in these systems was controlled primarily by the depth of the gravitational potential well in which they formed. The dashed line indicates our adopted color-magnitude relation for the GC systems of these protogalactic building blocks, each of which is assumed to have formed via a “monolithic” collapse. The dotted region shows the area occupied by galaxies that grow hierarchically via dissipationless agglomeration of these protogalactic fragments.

fragment, as it would appear today, if the subsequent evolution has been mostly passive. In the simulations, the mean color/metallicity of GCs belonging to each protogalactic fragment is determined using equation (4), with an assumed 1σ scatter of 0.03 mag (0.1 dex). The *internal* dispersion in color for each protogalactic fragment is also approximated as a Gaussian, with dispersion 0.09 mag (0.29 dex) based on the findings of Côté et al. (2000).

Finally, we adopt a constant GC specific frequency for all protogalactic fragments— $S_N \equiv 5 \pm 1$ at the present time—and neglect possible variations in S_N at the low- and high-mass ends of the galaxy distribution (see § 6). In the notation of McLaughlin (1999), this specific frequency corresponds to a GC formation efficiency of

$$\epsilon_{GC} = 0.29 \pm 0.06\% \quad (5)$$

by mass. This is consistent with the value of $\epsilon_{GC} = 0.26 \pm 0.05\%$ advocated by McLaughlin (1999) based on observations of about 100 early-type galaxies. The 20% uncertainty in our adopted values of S_N and ϵ_{cl} reflects the observed scatter about their means and has been included explicitly in our Monte Carlo simulations.

3.2. An Example

Before proceeding, we present a descriptive example of how the GC system of a galaxy that grows hierarchically through dissipationless mergers will evolve in the color-magnitude plane. Consider a protogalactic fragment, A, with absolute magnitude $M_V = -20$ mag and mass

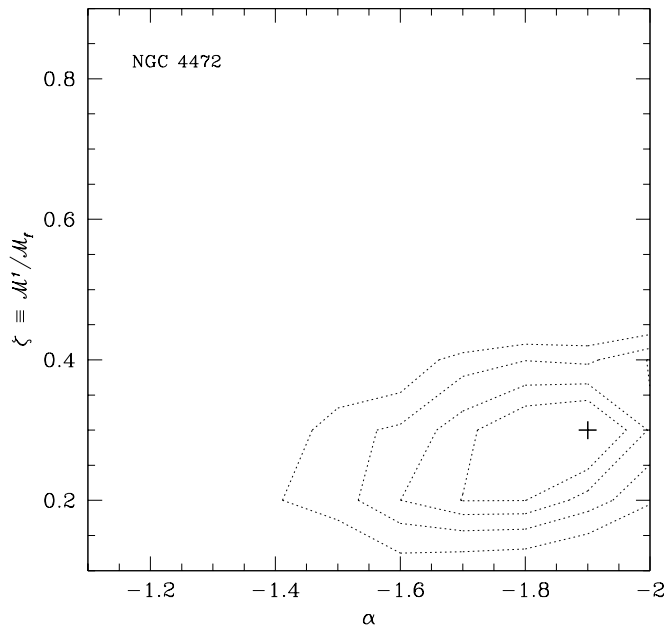


FIG. 2.—Confidence intervals for α and ζ , based on 5,000 Monte Carlo simulations of the metallicity distribution of globular clusters associated with the elliptical galaxy NGC 4472. In this notation, the slope of the protogalactic mass/luminosity function is denoted by α , while ζ is the ratio between the mass of the largest protogalactic fragment and the final mass of the galaxy. The contours denote 68%, 90%, 95%, and 99% confidence limits. The cross indicates the location in the α - ζ plane of the simulation that produced the best match to the observed distribution.

$M = 4 \times 10^{10} M_{\odot}$, that falls on the zero-age color-magnitude relation (i.e., Fig. 1, *dashed line*). According to equation (4), the unimodal GC system associated with this protogalactic fragment will have $\langle V-I \rangle = 1.14$ mag. First, suppose that this fragment merges with an identical fragment, producing an end product, C1, with $M_V = 20.75$ mag and a GC system having a single peak at $\langle V-I \rangle = 1.14$ mag. Alternatively, fragment A could accrete a population of 100 protogalactic fragments, B, each of which has $M_V = -15$ mag, and $\langle V-I \rangle = 0.865$ mag. But, by virtue of equation (5) and our assumed constant mass-to-light ratio, fragment A contributes the same number of GCs as the 100 smaller fragments combined. Thus, the GC systems of the final galaxy, C2, will have two distinct components (containing equal numbers of metal-rich and metal-poor GCs), and a mean color of $\langle V-I \rangle \simeq 1.00$ mag. A third possible end product, C3, is also shown in Figure 1. In this case, the galaxy was formed entirely through the agglomeration of (200) fragments of type B, so that the final GC system is unimodal, but with a metal-poor peak at $\langle V-I \rangle = 0.865$ mag.

The point of this simple exercise to emphasize that, once the “zero-age” color-metallicity is fixed, it is possible—through a suitable adjustment of the mass spectrum of the protogalactic fragments—to reproduce the GC systems of any galaxy whose GC system falls within the dotted region shown in Figure 1. This simple recipe for galaxy formation combines dissipationless mergers, which serve to move the galaxy to the right of the initial color-magnitude relation, with a dissipative, monolithic collapse scenario for the constituent protogalactic fragments. Our goal is to use the observed GC metallicity distribution for a specific galaxy and solve an inverse problem to determine the mass spec-

trum of protogalactic fragments that best matches the observed metallicity distribution.

3.3. Application

With equations (2) and (4) specified, it is a trivial matter to calculate analytically the metallicity distribution of a GC system, which arises from dissipationless mergers and accretions. In practice, such an approach is thwarted by the highly stochastic nature of hierarchical galaxy formation (e.g., Lacey & Cole 1993), particularly at the high-mass end of the protogalactic mass spectrum. Fortunately, this stochasticity can be used to reconstruct merger histories for individual galaxies since the fossil record of the largest protogalactic fragments is usually preserved in the final GC metallicity distribution.

To do so, we generate, for each galaxy in our sample, 50 simulated GC systems at each point over a 10×10 grid in (ζ, α) , where ζ is the ratio between the mass of the largest protogalactic fragment and the final mass of the galaxy,

$$\zeta = M^1/M_f, \quad (6)$$

and α is the slope of the protogalactic mass function. The (ζ, α) plane is sampled at $\zeta = 0.1, 0.2, \dots, 1.0$ and $\alpha = -1.1, -1.2, \dots, -2.0$. For each of the 5000 simulations per galaxy, we extract at random from the full GC system the same number of GCs as contained in the Kundu & Whitmore (2001) catalog, add the appropriate amount of measurement error to the simulated $(V-I)$ colors, and bin the actual and simulated data in an identical manner (see § 4.1). A goodness-of-fit statistic,

$$\chi^2 = \frac{1}{N_{\text{bin}} - 1} \sum_{i=1}^{N_{\text{bin}}} \frac{(N_{\text{obs},i} - N_{\text{sim},i})^2}{(N_{\text{obs},i} + N_{\text{sim},i})}, \quad (7)$$

is then calculated for each simulation, along with a mean χ^2 for each point on the 10×10 grid. The number of bins, N_{bin} , is chosen on a galaxy-by-galaxy basis as described in § 4.1. As an illustration of the method, Figure 2 shows a contour plot over this grid for one of the galaxies in our sample, NGC 4472. From these simulations, we deduce best-fit values of $\zeta = 0.30 \pm 0.05$ and $\alpha = -1.85 \pm 0.10$ (1σ uncertainties). The cross in Figure 2 shows the location in the (ζ, α) plane of the simulation which produced the best match to the observed GC metallicity distribution. These results are summarized in the final three columns of Table 1, which record the χ^2 for the best-fit simulation, along with the corresponding values of α and ζ and their 1σ uncertainties.

The mean simulated color of the GC systems in the sample is $\langle V-I \rangle_{\text{sim}} = 1.00$, while the mean difference between the observed and simulated GC color is $\langle V-I \rangle_{\text{obs}} - \langle V-I \rangle_{\text{sim}} = 0.00$ mag, with a standard deviation of 0.01 mag. We now turn our attention to a comparison of the detailed shapes of the observed and simulated GC color and metallicity distributions.

4. RESULTS

4.1. Metallicity Distributions

In this section, we compare the observed GC color and metallicity distributions with the best-fit models for each of our program galaxies. We follow the usual practice of presenting the results as histograms: i.e., as parametric representations of the underlying distributions. An optimal histogram bin width, h , is calculated on a case-by-case basis

according to the GC sample size and level of non-Gaussianity for each metallicity distribution. Specifically, we use the method of Scott (1992) and set the bin width at

$$h \simeq \frac{2.7\sigma\eta}{N_{\text{GC}}^{1/3}}, \quad (8)$$

where σ is the standard deviation of the distribution and η is a factor in the range $0.4 \lesssim \eta \lesssim 1$ related to the distribution's skewness. For our program objects, the bin widths range between $h \simeq 0.055$ mag for NGC 4649, and $h \simeq 0.138$ for NGC 4550; these values of h are comparable to the mean errors, $\sigma(V-I) = 0.08$ mag, of the measured GC colors. Note that this procedure differs from that of Kundu & Whitmore (2001), who opted to fix the bin width at a constant value of $h = 0.03$ mag, although N_{GC} varies by more than an order of magnitude among their program galaxies.

Figures 3–9 show the metallicity distributions for GCs belonging to the 28 galaxies listed in Table 1. The observed distributions are indicated by the filled circles, while the error bars show the Poisson uncertainties in each bin. For each galaxy, the best-fit model is indicated by the dashed curve, which has been binned in the same manner as the actual data. The excellent agreement between the observed and simulated distributions is noteworthy in light of the fact that, for the simple model considered here, the effects of just two free parameters, ζ and α , are explored. A more comprehensive exploration of parameter space might include possible mass-dependent variations in the GCs formation efficiency, the dynamical evolution of the GC systems, GC formation induced by the merger and accretion process, and the form of the intrinsic metallicity distribution in the protogalactic fragments. The first two processes were included in the Milky Way formation model discussed in Côté et al.

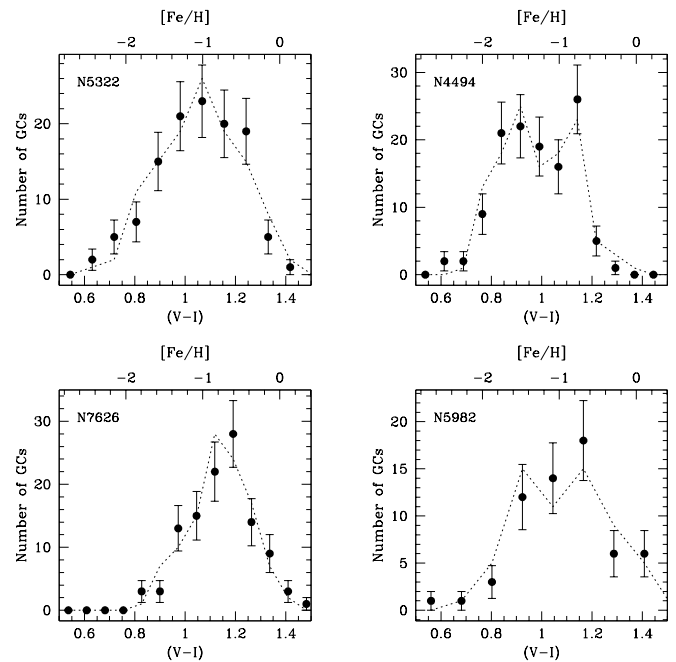


FIG. 4.—Same as in Fig. 3, except for NGC 5322, NGC 4494, NGC 7626, and NGC 5982.

(2000), but have been omitted here for the sake of simplicity. We note, however, that both the weak dependence of GC specific frequency on host galaxy luminosity (e.g., Durrell et al. 1996; Miller et al. 1998; McLaughlin 1999) and the preferential disruption of the more centrally concentrated metal-rich GCs in these galaxies, will serve to *increase* the ratio of metal-poor to metal-rich GCs. Including these effects in the simulations would give additional freedom to match the relative numbers of metal-rich and metal-poor GCs in these galaxies. To first order, these processes affect

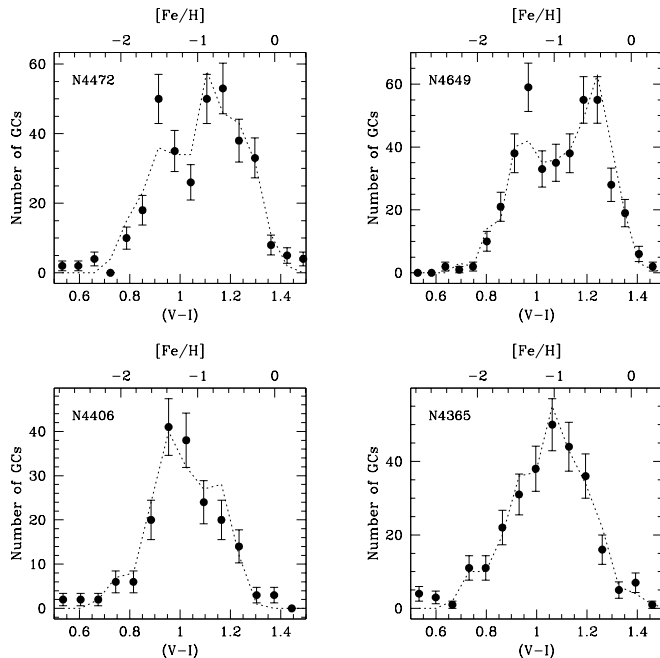


FIG. 3.—Color and metallicity distributions of globular clusters belonging to the early-type galaxies NGC 4472, NGC 4649, NGC 4406, and NGC 4365 (filled circles). The error bars show the Poisson uncertainties in each bin. The dashed curve shows the best-fit model for each galaxy, determined from 5000 Monte Carlo simulations spanning a 10×10 grid in (α, ζ) .

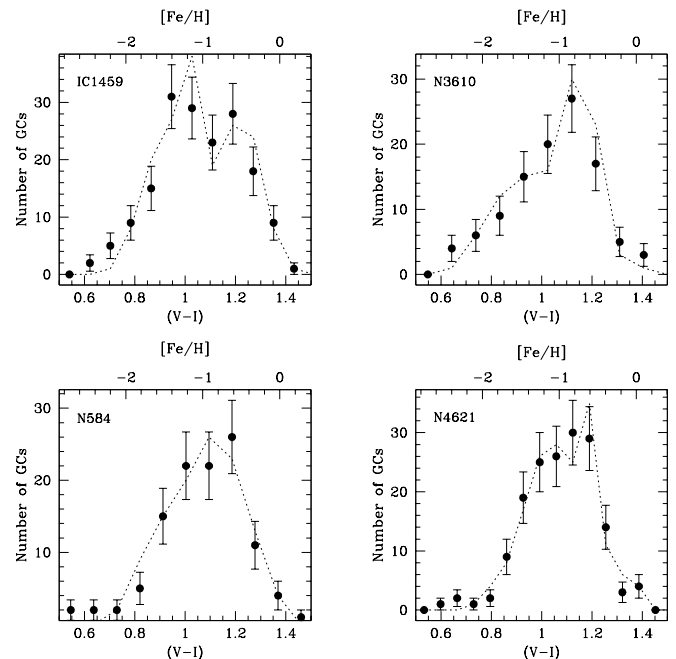


FIG. 5.—Same as in Fig. 3, except for IC 1459, NGC 3610, NGC 584, and NGC 4621.

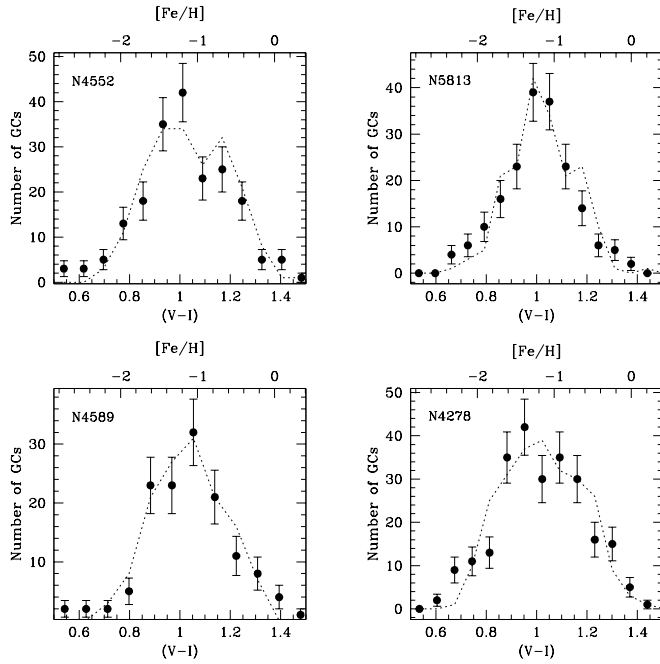


FIG. 6.—Same as in Fig. 3, except for NGC 4552, NGC 5813, NGC 4589, and NGC 4278.

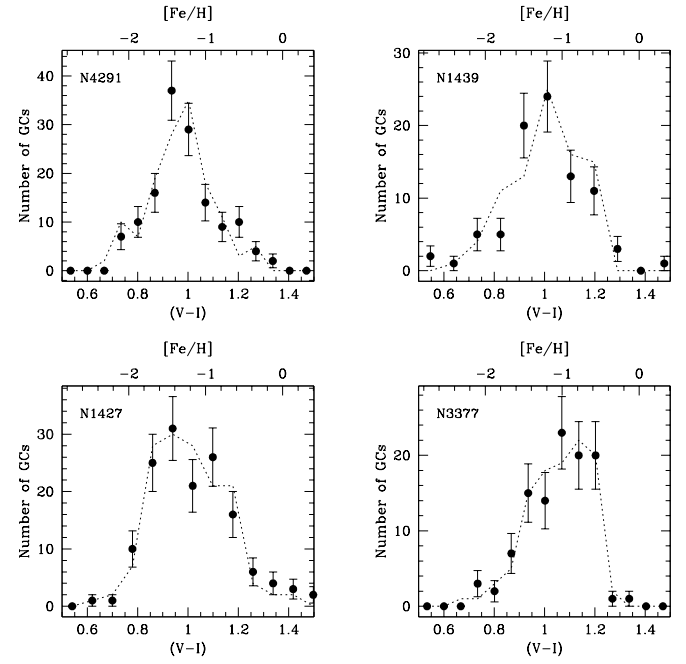


FIG. 8.—Same as in Fig. 3, except for NGC 4291, NGC 1439, NGC 1427, and NGC 3377.

the peak heights for the subsystems, and not their mean metallicities.

Figure 10 presents the same color-magnitude plane for GC systems that was shown in Figure 1. However, we now include the GC systems of the 28 galaxies listed in Table 1. Kundu & Whitmore (2001) classified each of these GC systems as either “certainly” bimodal, “likely” bimodal or unimodal. We adopt their classifications verbatim. For the 16 galaxies classified as certainly or likely bimodal, the peak color for the metal-rich and metal-poor GC systems

(according to KMM) are indicated by the filled squares and circles, respectively.² The filled triangles indicate the mean color and metallicity of the 12 unimodal GC systems. The open symbols show the median colors and metallicities of the GC systems in each of these galaxies based on 100

² The GC systems of NGC 3377 and NGC 584 are classified by Kundu & Whitmore (2001) as “likely” to be bimodal in their Table 1, but plotted as “certain” in their Fig. 5. We have assumed that the GC systems of both galaxies show statistically significant evidence of bimodality.

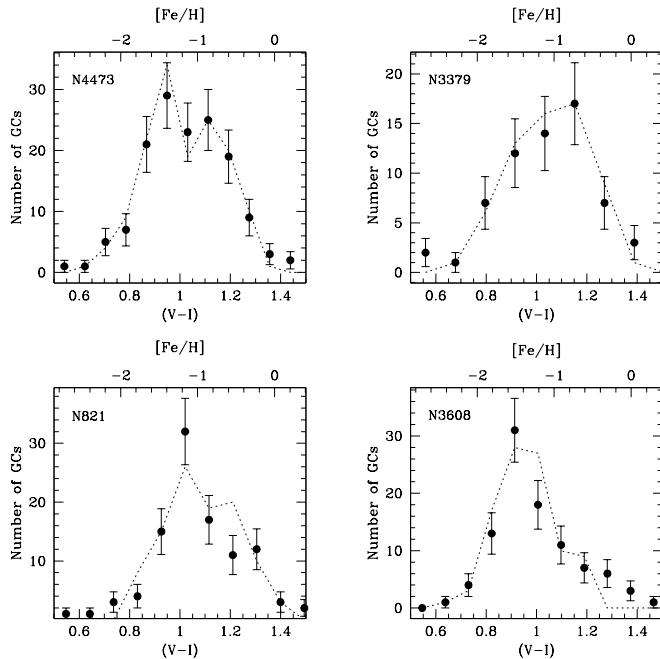


FIG. 7.—Same as in Fig. 3, except for NGC 4473, NGC 3379, NGC 821, and NGC 3608.

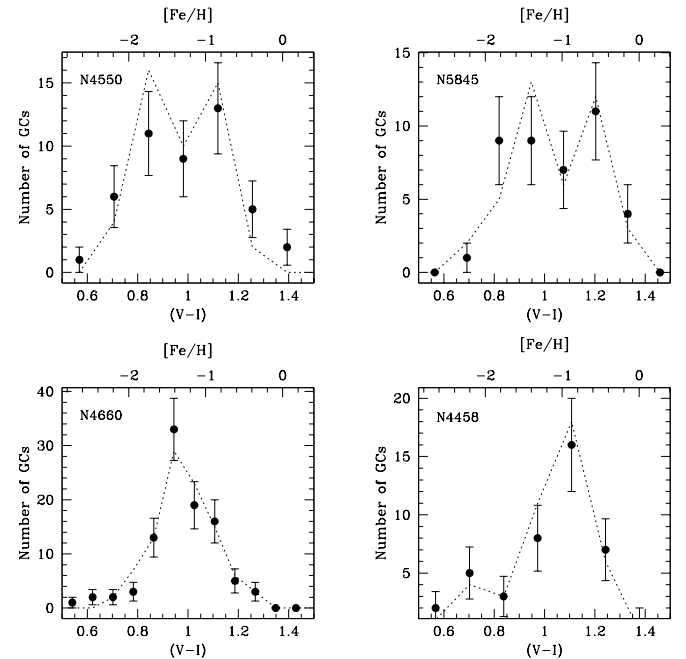


FIG. 9.—Same as in Fig. 3, except for NGC 4550, NGC 5845, NGC 4660, and NGC 4458.

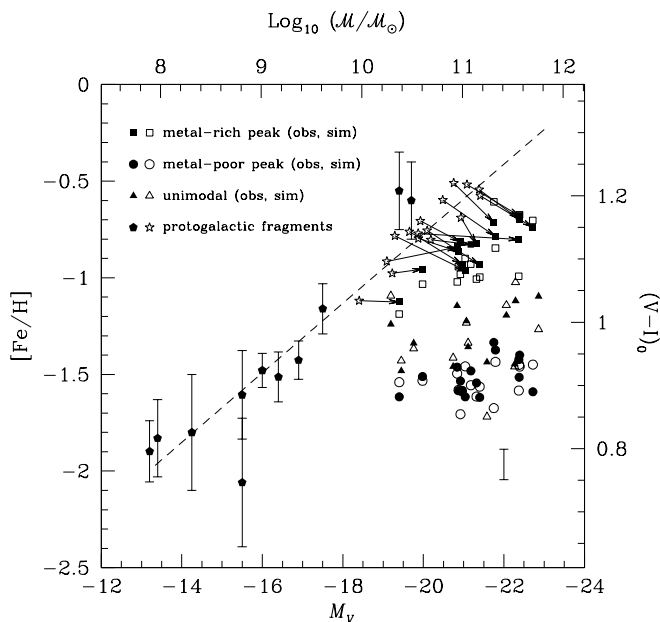


FIG. 10.—Mean color (metallicity) of globular cluster systems, plotted against galaxy magnitude (mass). The dashed line shows the “zero-age” relation between galaxy mass and globular cluster metallicity shown in Fig. 1 for unmerged protogalactic fragments: i.e., isolated galaxies of low and intermediate mass, and the bulge components of spiral galaxies (filled pentagons). The filled squares and circles show the observed colors for the metal-rich and metal-poor globular clusters in the 16 galaxies classified as bimodal by Kundu & Whitmore (2001). Open squares and circles indicate the median color of these components based on 100 simulations of the globular cluster metallicity distributions using the (α, ζ) values reported in Table 1. The filled and open triangles show the observed and simulated colors of globular clusters belonging to the 12 galaxies classified by Kundu & Whitmore (2001) as unimodal. The error bar in the lower right corner shows the 1σ scatter about these median values. For each galaxy with a bimodal metallicity distribution, a thin arrow connects the original position of the most massive protogalactic fragment (open stars) to the measured position of the metal-rich peak.

simulations using the best-fit values of ζ and α listed in Table 1. Simulations for the unimodal systems are indicated by the open triangles, while the open squares and open circles show the median colors for the metal-rich and metal-poor components in the bimodal systems (determined from the best-fitting double Gaussians). To illustrate the typical range in simulated GC color and metallicity, an error bar is included in the lower right corner of this figure, showing the 1σ dispersion in the colors and metallicities based on the simulations.

The simulations reproduce the observed GC colors and metallicities of not just the unimodal systems, but also of the metal-rich and metal-poor components in the bimodal GC systems. Likewise, the simulations reproduce the observed trend for the metal-poor peak in the bimodal GC systems to depend only weakly on host galaxy luminosity (Forbes, Brodie, & Grillmair 1997; Côté et al. 1998; Larsen et al. 2001) and, by definition, the clear correlation between metal-rich peak and host galaxy luminosity. This latter trend can be traced to the fact that the first-ranked protogalactic fragments: (1) themselves originate on the “zero-age” color-magnitude relation; and (2) contribute a significant fraction of the galaxy’s final mass. Indeed, for each galaxy classified by Kundu & Whitmore as bimodal, we show the initial location in the color-magnitude plane of the largest protogalactic fragment, determined from the best-fit simula-

tion for each galaxy (open stars). Thin arrows connect these initial positions to the locations of the metal-rich peak measured directly from the observed GC metallicity distribution. Note that, in a few cases, measurement errors and observational scatter (indicated by the error bar) cause the initial location in the color-magnitude plane to lie below the final location of the metal-rich peak. The filled pentagons show the GC systems of the same protogalactic fragments (i.e., dwarfs and spiral bulges) used to define the “zero-age” color-magnitude relation in Figure 1, reproduced as the dashed line in Figure 10. We conclude that the simple model considered here provides an adequate match to both the observed GC metallicity distributions and the final location of the GC systems in the color-magnitude plane.

4.2. Comparisons with Previous Results

On the basis of the same GC data analyzed here, Kundu & Whitmore (2001) claim that hierarchical models for galaxy formation are unviable. As Figures 3–10 demonstrate, this conclusion is not supported by their data.

Kundu & Whitmore (2001) made no attempt to simulate the GC color distributions expected in hierarchical formation scenarios, despite the fact that the implementation of such algorithms has been described in detail previously (e.g., Côté et al. 2000; Harris et al. 2000). Instead, they advocate a qualitative scenario in which GC formation occurs in multiple star formation episodes driven by mergers of gas-rich disk galaxies, although such models are currently not amenable to observational tests. They further note that some of the low-luminosity galaxies in their sample (e.g., NGC 1439, NGC 3377 and NGC 4660) are likely to have bimodal GC metallicity distributions and claim that this observation poses “a serious problem” for the hierarchical model. This claim is surprising since Côté et al. (2001) showed that hierarchical models were able to reproduce the bimodal GC metallicity distribution of the Galactic spheroid, which is several times fainter than NGC 1439, NGC 1427, and NGC 3377. Moreover, all of the low-luminosity galaxies having bimodal GC metallicity distributions fall within the region in Figure 1 that is expected to be occupied by galaxies which form hierarchically (§ 3.2). As Figures 3–9 attest, the observed diversity in the GC metallicity distributions and the bimodal nature of some low-luminosity ellipticals could arise naturally within the context of a simple hierarchical model.

Kundu & Whitmore (2001) also state that the success of the hierarchical model “is critically dependent on the second-order nature of [the metallicity-luminosity relation for] the systems being cannibalized.” However, this claim too is incorrect since the model distributions presented in Figures 3–9 are derived from a linear metallicity-luminosity relation (see § 3.1), not the second-order relation adopted by Côté et al. (1998) on these basis of preliminary data. While it is clearly important to further refine the metallicity luminosity relation for the GC systems of low- and intermediate-luminosity galaxies, the model described here is quite general, and our conclusions are unlikely to be changed by modifications to the metallicity-luminosity relation.

4.3. Protogalactic Mass Spectra

Having shown that hierarchical growth through dissipationless mergers and accretions offers a viable explanation for the diverse metallicity distributions of GC systems in early-type galaxies, we now examine the properties of the

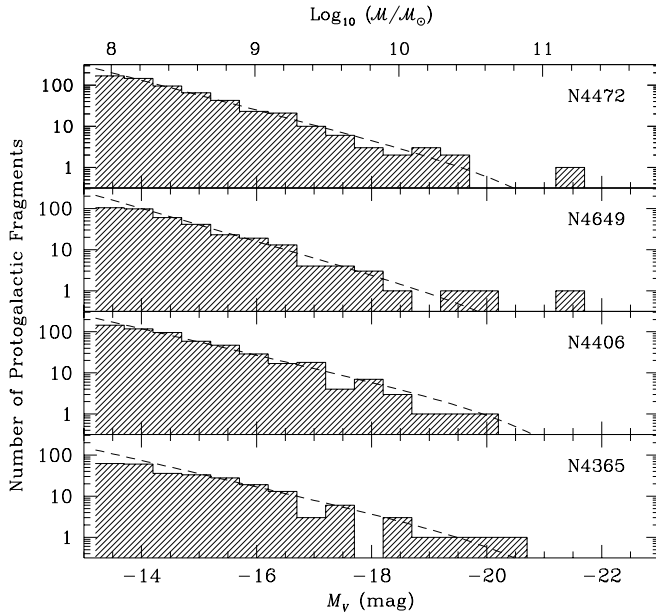


FIG. 11.—Mass and luminosity functions of protogalactic fragments for NGC 4472, NGC 4649, NGC 4406, and NGC 4365. The histograms show the distribution of protogalactic fragments for the best-fit models shown in Figure 3. The dashed line in each panel indicates the parent Schechter function from which the protogalactic fragments were drawn.

protogalactic fragments from which the galaxies may have been assembled. Figures 11–17 show protogalactic luminosity and mass functions for each galaxy, based on the simulation which matches the observed GC metallicity distribution. The shaded histogram in each panel shows the best estimate for the distribution of protogalactic fragments, while the dashed curve indicates the parent Schechter function from which the simulation was drawn. For all galaxies, the corresponding GC metallicity distributions are indicated by the dashed curves in Figures 3–9.

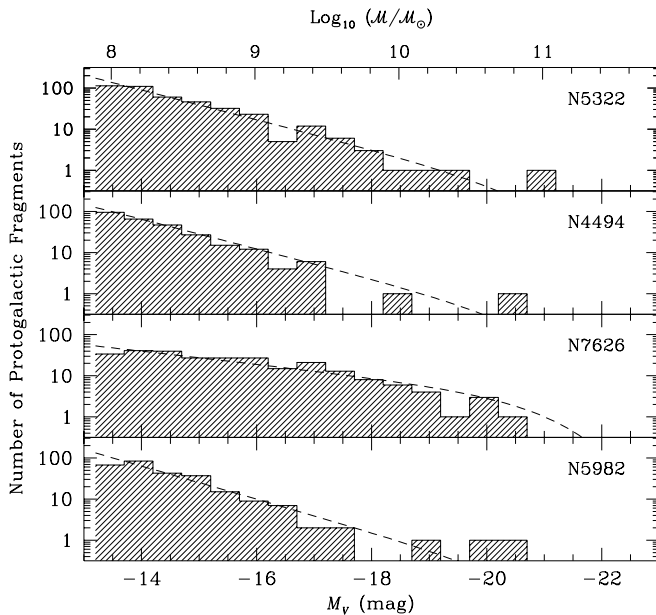


FIG. 12.—Same as in Fig. 11, except for NGC 5322, NGC 4494, NGC 7626, and NGC 5982.

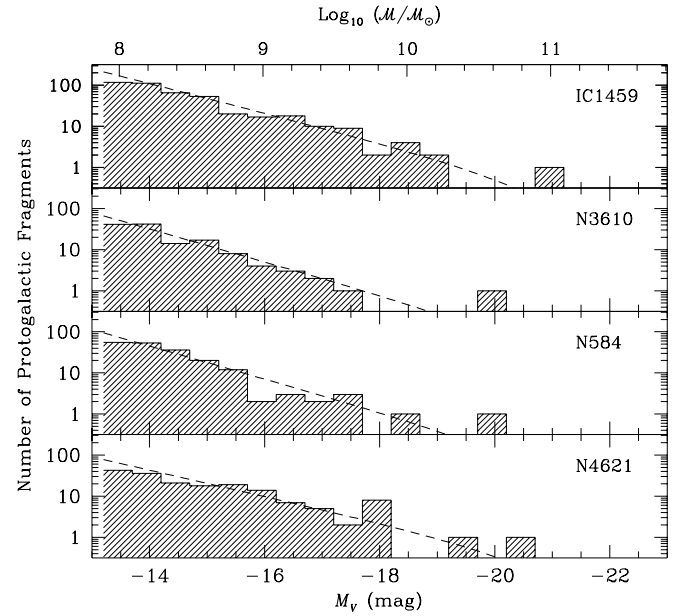


FIG. 13.—Same as in Fig. 11, except for IC 1459, NGC 3610, NGC 584, and NGC 4621.

A striking feature of the protogalactic luminosity and mass functions shown in Figures 11–17 is their steep slope. From Table 1, the average power-law exponent for the protogalactic luminosity and mass functions is $\langle\alpha\rangle = -1.88 \pm 0.03$ (mean error), with a standard deviation of $\sigma(\alpha) = 0.13$. This value is consistent with previous findings for NGC 4472 ($\alpha \sim -1.8$; Côté et al. 1998), the Milky Way ($\alpha \sim -2.0$; Côté et al. 2000) and M31 ($\alpha \sim -1.8$; Côté et al. 2000). In the context of hierarchical formation models, it is the apparent universality of this exponent which, when coupled with the fixed low-mass cutoff of the protogalactic luminosity function, conspires to produce the population of metal-poor GCs with $[\text{Fe}/$

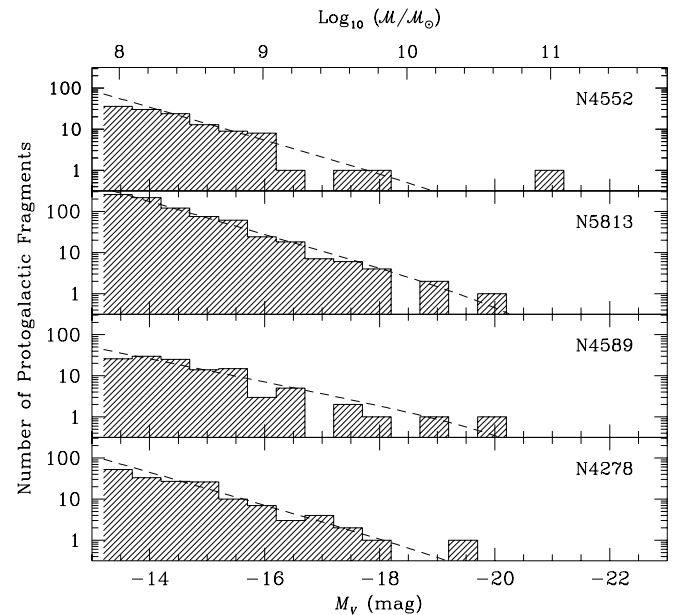


FIG. 14.—Same as in Fig. 11, except for NGC 4552, NGC 5813, NGC 4589, and NGC 4278.

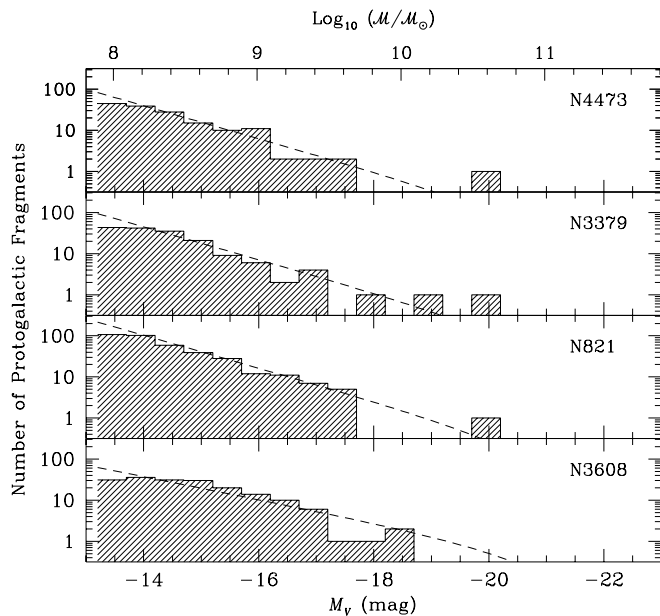


FIG. 15.—Same as in Fig. 11, except for NGC 4473, NGC 3379, NGC 821, and NGC 3608.

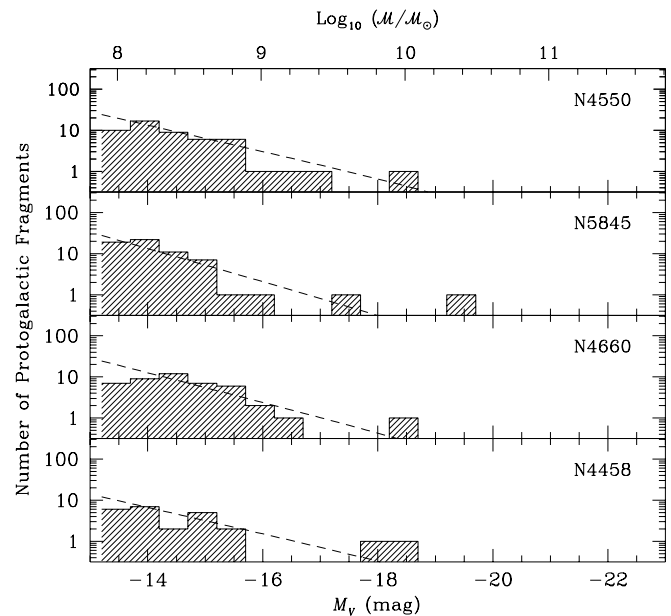


FIG. 17.—Same as in Fig. 11, except for NGC 4550, NGC 5845, NGC 4660, and NGC 4458.

H] ~ -1.2 dex that are present in virtually every large galaxy studied to date (e.g., Ashman & Bird 1993; Brodie, Larsen, & Kissler-Patig 2000). As the same time, the observed diversity of GC metallicity distributions arises from the stochastic fluctuations about this “universal” protogalactic mass spectrum, particularly at the high-mass end. By virtue of their large mass, these fragments contribute the bulk of the metal-rich GCs associated with the final galaxy.

From Table 1, we see that there is a fairly wide range in the properties of the most massive protogalactic fragments. On average, the most massive fragment contributes a fraction $\langle \zeta \rangle = 0.25 \pm 0.03$ (mean error) of the galaxy’s final mass, with a standard deviation of $\sigma(\zeta) = 0.14$. For some

galaxies, such as NGC 4406, the contribution of the largest fragment amounts to no more $\sim 10\%$ of the final mass, while in NGC 4458, as much as 70% of the final mass may have arisen in the dissipational collapse of the largest protogalactic fragment. For NGC 4472, we find a best-fit value of $\zeta = 0.30 \pm 0.05$ (mean error), which compares favorably with the value of $\zeta \sim 0.35$ estimated by Côté et al. (1998) using ground-based observations of its GC system carried out in a different filter system (i.e., CT_1 photometry from Geisler, Lee, & Kim 1996), and using an alternative color-magnitude relation.

Recent studies have concluded that approximately 50% of bright, early-type galaxies show evidence for bimodal color distributions (Gebhardt & Kissler-Patig 1999; Larsen et al. 2001; Kundu & Whitmore 2001), so it is of interest to ask how often the simulations yield a metallicity distribution that is bimodal at a statistically significant level. Unfortunately, the answer to this question depends rather sensitively on the properties of each data set used to assess the level of bimodality. To understand why this is so, consider Figure 18, which shows the metallicity distribution for a representative program galaxy, NGC 5322. For the purposes of illustration, the solid curve shows the (normalized) metallicity distribution corresponding to the protogalactic mass function plotted in the upper panel of Figure 12, where the intrinsic dispersion in metallicity for each protogalactic fragment is taken to be 0.01 dex. As discussed in § 3.1 and in Côté et al. (2000), actual fragments are likely to have had intrinsic dispersions much larger than this, but this extreme example serves to illustrate the complex nature of the underlying metallicity distribution, and demonstrates the dangers of interpreting multimodal metallicity distributions as *prima facie* evidence for multiple bursts of GC formation. The remaining curves show this same (renormalized) distribution after smoothing with Gaussians having dispersions of 0.1, 0.2, 0.3, and 0.4 dex (intended to represent the combined effects of an intrinsic metallicity dispersion and observational errors). This last distribution is, like the observed distribution, ostensibly unimodal in nature

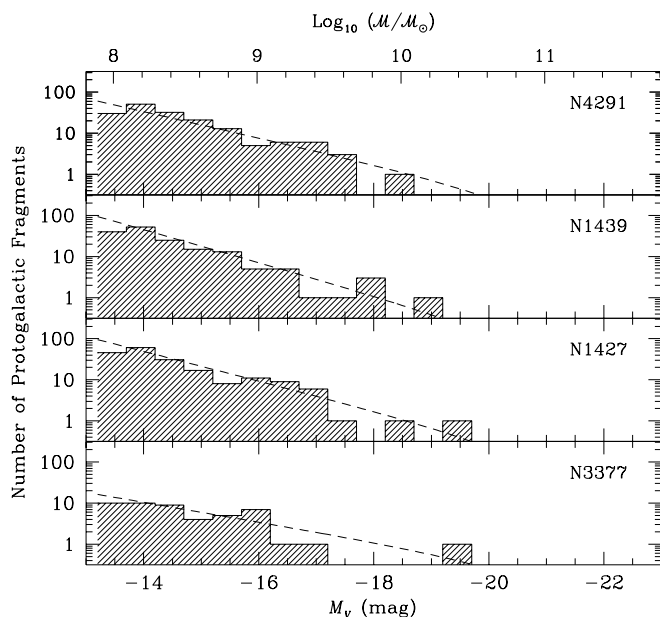


FIG. 16.—Same as in Fig. 11, except for NGC 4291, NGC 1439, NGC 1427, and NGC 3377.

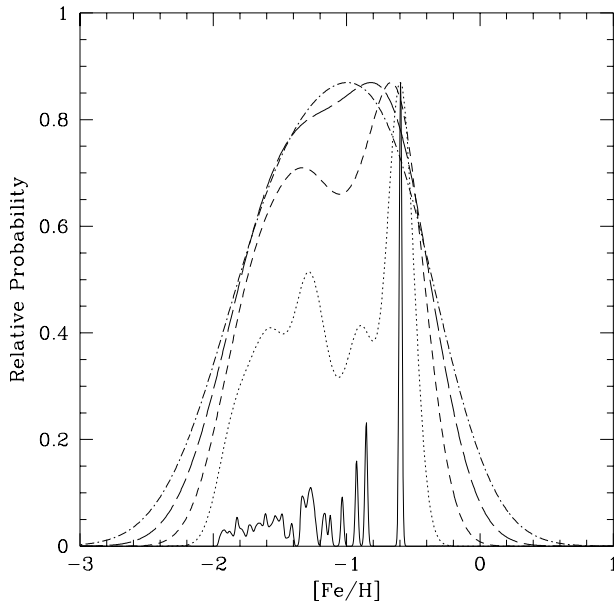


FIG. 18.—Simulated metallicity distribution for a representative galaxy, NGC 5322, assuming that the intrinsic metallicity dispersion of each protogalactic fragment is 0.01 dex (solid curve). The remaining curves show this same distribution after smoothing with Gaussians having dispersions of 0.1, 0.2, 0.3, and 0.4 dex.

(Kundu & Whitmore 2001), but this is mainly a consequence of the intrinsic metallicity dispersion (~ 0.3 dex) for the protogalactic fragments, and the ~ 0.3 dex dispersion associated with metallicity measurements derived from $(V-I)$ colors having a precision of roughly 0.1 mag. Thus, establishing the frequency of bimodality depends rather sensitively on the precision of metallicity measurements (and on other factors including the total luminosity of the final galaxy and its detailed merger tree).

5. IMPLICATIONS FOR THE MISSING SATELLITE PROBLEM

As mentioned in § 1, one of the most troubling problems facing CDM models on small scales is the so-called missing satellite problem. Simply stated, the number of low-mass dark halos predicted by CDM models exceeds the observed number of dwarf galaxies by factors of tens, or even hundreds (e.g., Kauffmann et al. 1993; Klypin et al. 1999; Moore et al. 1999). Is it possible to explain the underabundance of dwarf galaxies in the local universe, and at the same time retain the basic framework of CDM models?

Figure 19 shows the ensemble spectrum of protogalactic fragments in our sample: i.e., summed over all 28 galaxies (filled circles). As with the individual galaxies, the composite mass function is found to follow a power-law behavior, $n(M) \propto M^\alpha$, with exponent $\alpha \simeq -2$. While this mass function is much steeper than the local galaxy luminosity function (i.e., Pritchet & van den Bergh 1999; Folkes et al. 1999; Blanton et al. 2001), it is nevertheless in remarkable agreement with the mass spectrum of dark matter halos predicted by CDM models of structure formation; the dotted line in Figure 19 shows the analytical approximation, $n(M) \propto M^{-2}$, for the mass spectrum of dark matter halos in the N -body simulations of Moore et al. (1999). *In short, we find evidence for a disrupted population of dwarf-sized protogalactic fragments in each of our program objects, whose numbers and masses closely resemble those of the predicted population of “missing” satellite galaxies.*

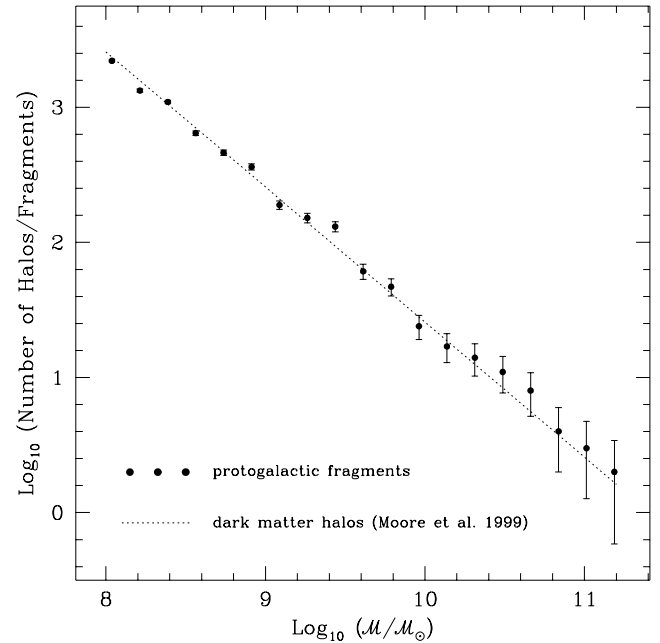


FIG. 19.—Comparison of the halo mass function measured from cosmological N -body simulations (dotted line) with the mass spectrum of protogalactic fragments inferred from the 28 globular cluster systems studied here (filled circles). Following Moore et al. (1999), we express the mass function of dark matter halos as $n(M) \propto M^{-2}$, equivalent to $n(\log M) \propto (\log M)^{-1}$.

This finding may have important consequences for the various models that have been advanced as possible solutions to the missing satellite problem. Such a disrupted population is, in fact, predicted by models that account for the missing satellites by suppressed gas accretion in low-mass halos after the epoch of reionization due the presence of a strong photoionizing background (e.g., Rees 1986; Thoul & Weinberg 1996; Bullock et al. 2000). A disrupted component of this sort is also expected in models which seek to explain the missing satellite problem through self-interacting CDM (e.g., Spergel & Steinhardt 2000; Davé et al. 2001). By contrast, a disrupted component is not expected in models that explain the underabundance of dwarf galaxies through an ab initio reduction in small scale power (e.g., Kamionkowski & Liddle 2000) or by suppressing the formation of low-mass halos via warm dark matter (e.g., Colín, Avila-Reese & Valenzuela 2000; Sommer-Larsen & Dolgov 2001). Thus, these models appear to be inconsistent with the observed metallicity distributions of GCs in galaxies at $z \sim 0$ since the same low-mass halos whose formation is suppressed in these scenarios are actually required to explain the GC metallicity distributions of luminous galaxies in hierarchical cosmologies.

6. SUMMARY AND CONCLUSIONS

We have described a technique for simulating the metallicity distributions of GCs belonging to galaxies that grow hierarchically through dissipationless mergers and accretions. Applying the model to the GC systems of 28 early-type galaxies for which high quality *HST* data are available demonstrates such a mechanism is capable of explaining quantitatively the observed diversity in extragalactic GC systems. Thus, claims that the metallicity distributions of GCs in early-type galaxies are inconsistent with a hierarchical origin (Kundu & Whitmore 2001) are unsubstantiated.

Progalactic mass spectra for the sample of early-type galaxies considered here reveal a striking similarity: they appear to follow a power-law distribution in mass, with $n(M) \propto M^{-2}$. This mass spectrum is indistinguishable from the mass spectrum of dark matter halos predicted by CDM models, and thus has an important implication for the missing satellite problem (Klypin et al. 1999; Moore et al. 1999). Specifically, we find evidence from the GC systems of the galaxies examined here for a disrupted population of dwarf-sized protogalactic fragments whose numbers and masses closely resemble those of the predicted population of missing satellite galaxies.

If the basic scenario outlined here is correct (i.e., the early formation of GCs in low- and intermediate-mass halos after a rapid period of mass-dependent chemical enrichment, followed by the agglomeration of these halos into the main body of the galaxy), then there may be some interesting observational consequences of this picture. For instance, if most of the low-mass dark matter halos predicted by CDM models have indeed been rendered undetectable as a result of disruption and the suppression of gas accretion after reionization, as suggested by Bullock et al. (2000), then some fraction of the original halo population may survive as “dark galaxies” (see, e.g., Klypin et al. 1999 and refer-

ences therein). Precise estimates for the redshift of GC formation are not yet available, but current evidence seems to favor formation at $z \gtrsim 7$ (see Gnedin et al. 2001), close to the expected edge of the epoch of reionization (Djorgovski et al. 2001; Becker et al. 2001; Barkana 2001). This raises the possibility that some of these putative “dark galaxies,” which have experienced little or no star formation, might nevertheless have managed to form GCs. Interestingly, there is some evidence that the number of GCs per unit host galaxy luminosity increases toward fainter systems, at least among dE,N galaxies (Durrell et al. 1996; Miller et al. 1998). Searches of extragalactic GC systems for compact, dynamically bound groupings of GCs—presumably metal-poor in nature and not associated with an identifiable satellite galaxy—might prove interesting.

We thank Arunav Kundu for providing the GC photometry used in the analysis, and an anonymous referee for helpful comments. M. J. W. was supported by NSF grant AST 00-71149. This research has made use of the NASA/IPAC Extragalactic Database (NED), which is operated by the Jet Propulsion Laboratory, California Institute of Technology, under contract with the National Aeronautics and Space Administration.

REFERENCES

- Ashman, K. A., & Bird, C. M. 1993, *AJ*, 106, 2281
 Bahcall, N., Ostriker, J. P., Perlmutter, S., & Steinhardt, P. J. 1999, *Science*, 284, 1481
 Barkana, R. 2001, *NewA*, submitted (astro-ph/0108431)
 Becker, R. H., et al. 2001, *AJ*, in press (astro-ph/0108097)
 Beasley, M. A., Sharples, R. M., Bridges, T. J., Hanes, D. A., Zepf, S. E., Ashman, K. M., & Geisler, D. 2000, *MNRAS*, 318, 1249
 Blanton, M. R., et al. 2001, *AJ*, 121, 2358
 Bruzual, G., & Charlot, S. 1993, *ApJ*, 405, 538
 Brodie, J. P., Larsen, S. S., & Kissler-Patig, M. 2000, *ApJ*, 543, L19
 Bullock, J. S., Kravtsov, A. V., & Weinberg, D. H. 2000, *ApJ*, 539, 517
 Buonanno, R., Corsi, C. E., Zinn, R., Fusi Pecci, F., Hardy, E., & Suntzeff, N. B. 1998, *ApJ*, 501, L33
 Burstein, D., & Heiles, C. 1984, *ApJS*, 54, 33
 Cen, R. 2001, *ApJ*, 118, 406
 Cohen, J. G., Blakeslee, J. P., & Rhyzov, A. 1998, *AJ*, 115, 2356
 Colin, P., Avila-Reese, V., & Valenzuela, O. 2000, *ApJ*, 542, 622
 Côté, P. 1999, *AJ*, 118, 406
 Côté, P., Marzke, R. O., & West, M. J. 1998, *ApJ*, 501, 554
 Côté, P., Marzke, R. O., West, M. J., & Minniti, D. 2000, *ApJ*, 533, 869
 Davé, R., Spergel, D. N., Steinhardt, P. J., & Wandelt, B. D. 2001, *ApJ*, 547, 574
 Djorgovski, S. G., Castro, S., Stern, D., & Mahabal, A. A. 2001, *ApJ*, 560, L5
 Durrell, P., Harris, W. E., Geisler, D., & Pudritz, R. 1996, *AJ*, 112, 972
 Faber, S. M. 1973, *ApJ*, 179, 423
 Flores, R. A., & Primack, J. R. 1994, *ApJ*, 427, L1
 Folkes, S., et al. 1999, *MNRAS*, 308, 459
 Forbes, D. A., Brodie, J. P., & Grillmair, C. J. 1997, *AJ*, 113, 1652
 Gebhardt, K., & Kissler-Patig, M. 1999, *AJ*, 118, 1526
 Geisler, D., Lee, M. G., & Kim, E. 1996, *AJ*, 111, 1529
 Gnedin, O. Y., Lahav, O., & Rees, M. J. 2001, *Nature*, submitted (astro-ph/0108034)
 Goodman, J. 2000, *NewA*, 5, 103
 Harris, G. L. H., Poole, G. B., & Harris, W. E. 1998, *AJ*, 116, 2866
 Harris, W. E. 2000, in *Star Clusters*, Saas-Fee Advanced Course 28 (Berlin: Springer)
 Harris, W. E., Kavelaars, J. J., Hanes, D. A., Hesser, J. E., & Pritchet, C. J. 2000, *ApJ*, 533, 137
 Ibata, R., Gilmore, G., & Irwin, M. J. 1994, *Nature*, 370, 194
 Kamionkowski, M., & Liddle, A. R. 2000, *Phys. Rev. Lett.*, 84, 4525
 Kauffmann, G., White, S. D. M., & Guiderdoni, B. 1993, *MNRAS*, 264, 201
 Kissler-Patig, M., Brodie, J. P., Schroder, L. L., Forbes, D. A., Grillmair, C. J., & Huchra, J. P. 1998, *AJ*, 115, 105
 Klypin, A. A., Kravtsov, A. V., Valenzuela, O., & Prada, F. 1999, *ApJ*, 522, 82
 Kormendy, J., et al. 1997, *ApJ*, 482, L139
 Kundu, A., & Whitmore, B. C. 2001, *AJ*, 121, 2950
 Lacey, C., & Cole, S. 1993, *MNRAS*, 262, 627
 Larsen, R. B. 1988, in *IAU Symp.* 126, *Globular Cluster Systems in Galaxies*, ed. J. E. Grindlay & A. G. D. Philip (Dordrecht: Reidel), 311
 Larsen, S. S., Brodie, J. P., Huchra, J. P., Forbes, D. A., & Grillmair, C. J. 2001, *ApJ*, 121, 2974
 Layden, A. C., & Sarajedini, A. 1997, *ApJ*, 486, L107
 Lee, M. G., & Kim, E. 2000, *AJ*, 120, 260
 Mateo, M. 1998, *ARA&A*, 36, 435
 McLaughlin, D. E. 1999, *AJ*, 117, 2398
 Miller, B. W., Lotz, J. M., Ferguson, H. C., Stiavelli, M., & Whitmore, B. C. 1998, *ApJ*, 508, L133
 Minniti, D. 1995, *AJ*, 109, 1663
 Moore, B., Ghinga, S., Governato, F., Lake, G., Quinn, T., Stadel, J., & Tozzi, P. 1999, *ApJ*, 524, 19
 Pearce, F. R., Jenkins, A., Frenk, C. S., White, S. D. M., Thomas, P. A., Couchman, H. M. P., Peacock, J. A., & Efstathiou, G. 2001, *MNRAS*, 326, 649
 Pritchet, C. J., & van den Bergh, B. 1999, *PASP*, 118, 883
 Prugniel, P., & Simien, F. 1996, *A&A*, 309, 749
 Puzia, T. H., Kissler-Patig, M., Brodie, J. P., & Huchra, J. P. 1999, *AJ*, 118, 2734
 Rees, M. J. 1986, *MNRAS*, 218, 25
 Riotto & Tkachev 2000, *Phys. Lett. B*, 484, 177
 Sakai, S., et al. 2000, *ApJ*, 529, 698
 Schechter, P. 1976, *ApJ*, 203, 297
 Schlegel, D. J., Finkbeiner, D. P., & Davis, M. 1998, *ApJ*, 500, 525
 Scott, D. W. 1992, *Multivariate Density Estimation* (New York: Wiley)
 Sellwood, J. A., & Kosowsky, A. 2002, in *ASP Conf. Ser.* 240, *Gas and Galaxy Evolution*, ed. J. E. Hibbard, M. P. Rupen & J. H. van Gorkom (San Francisco: ASP), in press (astro-ph/0009074)
 Sommer-Larsen, J., & Dolgov, A. 2001, *ApJ*, 551, 608
 Spergel, D. N., & Steinhardt, P. J. 2000, *Phys. Rev. Lett.*, 84, 3760
 Thoul, A. A., & Weinberg, D. H. 1996, *ApJ*, 465, 608
 Tonry, J. L., Dressler, A., Blakeslee, J. P., Ajhar, E. A., Fletcher, A. B., Luppino, G. A., Metzger, M. R., Moore, C. B. 2001, *ApJ*, 546, 681
 van den Bergh, S. 2001, *PASP*, 112, 932
 Whitmore, B. C., & Schweizer, F. 1995, *AJ*, 109, 960
 Worthey, G. 1994, *ApJS*, 95, 107